MEASUREMENT DRIFT IN 3-HOLE YAW PRESSURE PROBES FROM 5 MICRON SAND FOULING AT 1050° C

EDWARD J TURNER

Thesis Submitted To The Faculty Of Virginia Polytechnic Institute And State University In Partial Fulfillment Of The Requirements For The Degree Of

Master of Science
In
Mechanical Engineering

Wing F. Ng (Chair)
Clinton L. Dancey
Gary R. Pickrell
Kevin T. Lowe

On June 28, 2018
Blacksburg Va

Keywords: Turbo machinery, Sand Fouling, Pressure Probes

MEASUREMENT DRIFT IN 3-HOLE YAW PRESSURE PROBES FROM 5 MICRON SAND FOULING AT 1050° C

EDWARD J TURNER

ABSTRACT

3-hole pressure probes are capable of accurately measuring flow angles in the yaw plane. These probes can be utilized inside a jet engine hot section for diagnostics and flow characterization. Sand and other particulate pose a significant risk to hot section components and measurement devices in gas turbine engines. The objective of this experiment was to develop a better understanding of the sensitivity of experimental 3-hole pressure probe designs to engine realistic sand fouling. In this study, Wedge, Cylindrical, and Trapezoidal probes were exposed to realistic hot section turbine environments of 1050°C at 65-70 m/s. 0-5 micron Arizona Road Dust(ARD) is heated under these conditions and used to foul the yaw probes. The sand deposited on the probe was observed to peel off the probe in thin sheets during ambient cool down.

Sand fouling was assessed using a stereoscope and digital camera. Probe calibrations were performed in an ambient temperature, open air, calibration jet to mimic engine cold start conditions at Mach numbers of 0.3 and 0.5. Yaw coefficients were calculated for each probe using probe pressure and jet dynamic pressure readings. These coefficients were used to develop calibration curves for each probe initially, and again for every fouling test. Each probe performed differently, but the trends showed that the sand fouling had little impact on the probe error at Mach 0.3, and a slightly increased effect on the probe error at Mach 0.5. The experiment showed that when flow direction was determined using a true dynamic pressure reading from the jet, the probes were able to accurately measure flow direction even after being significantly sanded, some probes holes being over 50% blocked by sand accumulation.

Accelerated erosion testing showed that the trapezoidal yaw probe was by far the most sensitive to sand accumulation, followed by the cylindrical probes, and the least sensitive was the wedge probe. A yaw angle range of interest was chosen to ±10°of yaw. The least errors from the Yaw Coefficient, as defined in this report, were found to be in the Trapezoidal and Perpendicular probe configurations. The least error found in the wedge probe.

MEASUREMENT DRIFT IN 3-HOLE YAW PRESSURE PROBES FROM 5 MICRON SAND FOULING AT 1050° C

EDWARD J TURNER

GENERAL AUDIENCE ABSTRACT

3-hole pressure probes are used to measure the speed and direction of air and other fluid flows. These probes can be used inside an active jet engine to measure aspects of the airflow inside the engine during flight. One risk to aircraft engines is sand being ingested into the engine. This can cause significant damage to the engine as well as the hardware inside the engine. The objective of this experiment will be to determine how sand accumulation affects the performance of these probes. The experiment involved sanding the probes in a hot jet, then placing them in front of a room temperature air jet to take measurements. A microscope was used to determine how much sand was on the holes of the probe. Sand was observed to peel off naturally, as the probe cooled from the hot jet. Sand was also noticed to break off during the room temperature jet.

The experiment showed that when the Jet pressures was measured from inside the jet, the probes were able to accurately measure flow direction even after being significantly sanded, <50% of the holes being blocked by sand. Of all the probes tested, the Wedge probe performed the best, though a close second was the Trapezoidal probe.

MEASUREMENT DRIFT IN 3-HOLE YAW PRESSURE PROBES FROM 5 MICRON SAND FOULING AT 1050° C

EDWARD J TURNER

ACKNOWLEDGEMENTS

I would like to start by acknowledging the tremendous amounts of love, support, and positivity I received from my support network of friends, family, and loved ones. I would not have been able to complete this body of work without your guidance and support. Special thanks to my Mother and Father for constantly encouraging me. And the greatest thanks of all to my Lord and Savior Jesus Christ for giving me life, passion, and the drive to finish this tremendous adventure.

I would like to especially thank my dedicated research team: Matt Bogdan, Tyler O'Connel, Daniel VanHout, Kavi Muraleetharan, Smriti Kandel, James Ramser, Ansh Kapoor, Elizabeth Horley, and Tyler Jones.

Thank you to my labmates: Andrew Boulanger, Renzo LaRosa, and Vy Nguyen.

Table of Contents

List of Figures

List of Tables

MEASUREMENT DRIFT IN 3-HOLE YAW PRESSURE PROBES FROM 5 MICRON SAND FOULING AT 1050° C

Edward Turner, Matt Bogdan, Tyler O'Connell
Wing F. Ng
Virginia Tech, Mechanical Engineering Blacksburg,
Virginia, United States of America

Richard Stevenson, James Roberts, Loren Crook
Rolls-Royce PLC
Derby, United Kingdom
Rolls-Royce Corporation
Indianapolis, Indiana, USA

NOMENCLATURE

A_{Clean}	Clean probe clearance area
A_{Clear}	Fouled probe clearance area
ARD	Arizona road dust
BLR	Blockage ratio
C_{yaw}	Yaw Coefficient
Cyl	Cylindrical probe
Daq	Data Acquisition System
FS	Full Scale
ISO	International Organization for Standardization
M	Mach number
MP	Mega Pixel
NW	30° Wedge probe
P_S	Static pressure
P_T	Stagnation pressure
P_1	Center pressure hole
S_2	Right pressure hole
S_3	Left pressure hole

Symbols

⊥	Perpendicular

INTRODUCTION

Pressure probes have been used in the turbomachinery field for centuries and are still an essential component of flow measurement today. The traditional 2-hole pitot-static probe is able to measure stagnation and static pressures to determine flow velocities. Three or more-hole pressure probes have the added capability of measuring flow direction in the yaw and pitch planes, depending on the number of holes. 3-hole yaw probes are limited to measuring flow direction in the yaw plane. Yaw probes are useful in turbomachinery to measure flow pressures and flow directions for engine diagnostics.

Recent interest has increased in understanding the effect of airborne particulate fouling on engine components. In-air particulates can cause significant damage to engine hardware and measurement components, including pressure probes, during operation. This deposition is particularly of interest in regions downstream of the combustor of the gas turbine engine. Modern engines are equipped to filter out particulate greater than 75 μm in diameter [1]. Smaller particles however <10μm [2], like airborne sand and volcanic ash, and are known to pass through the combustion chamber and into the hot section of the engine. In the combustion chamber, gas temperatures often exceed the melting points of many of the particulates. This softens or melts the particulates, which leads to adhesion and erosion on valuable hot section hardware and probes. Particulate deposition is attributed to multiple modes of catastrophic failure in hot section turbine components. Research has been thoroughly conducted to better understand and model particulate deposition on turbine blades, inlet guide vanes, coolant channels, and other hot section hardware.

Much of the previous relevant research is focused on total blockage of pressure probes fixed outside of a turbomachine. These focus on the effects and mitigation of complete Pitot Probe blockage from icing, coal ash, dust particulate, etc. [3]. If the stagnation port is completely blocked, the probe measurement will be locked at the pressure the probe was blocked at. The unreliable airspeeds calculated from blocked probes have led to a multitude of aircraft failures. There is still much to learn about the effects of partial blockages from turbine inlet conditions on the performance of flow directional probes. The present study focuses on the effects of hot sand fouling and partial blockage on 3-hole pressure probes in the hot section of the gas turbine.

BACKGROUND

3-Hole Yaw Probe Description

There are many different geometries of 3-hole yaw probes. Commonly used geometries include: Cobra, Wedge, Cylindrical, and Pyramidal probes. The Wedge, Cylindrical, and Pyramidal shaped probes were chosen for this sand fouling study. Five sets of 3-hole configurations were selected, as shown in Table 1. Figure 1 shows a CAD rendering of the yaw probes. The convention for referencing the three holes is as follows, looking directly at the probe holes: the center hole is P1, the hole to the right side is S2, and the hole to the left side is S3. The P1 hole functions as the stagnation pressure tap, while the S2 and S3 holes are static pressure taps.

The Wedge Probe is a 30° nickel alloy wedge probe. The Wedge probe had both perpendicular holes and parallel holes machined into it. The perpendicular set has static ports(S2,S3) cut perpendicular to the surface of the wedge. The parallel static ports(S2,S3) are machined directly into the probe, parallel to the wedge axis. For both configurations, the center hole is cut parallel to the axis of flow, directly onto the blade of the wedge.

The Cylindrical Probe has 2 sets of cylindrical yaw configurations, and 1 Trapezoidal configuration. Cylindrical configuration 1, referred to as CYL 45° is a 3-hole cylindrical probe with static pressure holes(S2,S3) cut at 45° angles from the center hole. The second cylindrical configuration, referred to as CYL 55°, has static holes(S2,S3) cut at 55° angles. The trapezoidal head is a trapezoidal probe, with static ports(S2,S3) machined perpendicular to 45° angle tapers.

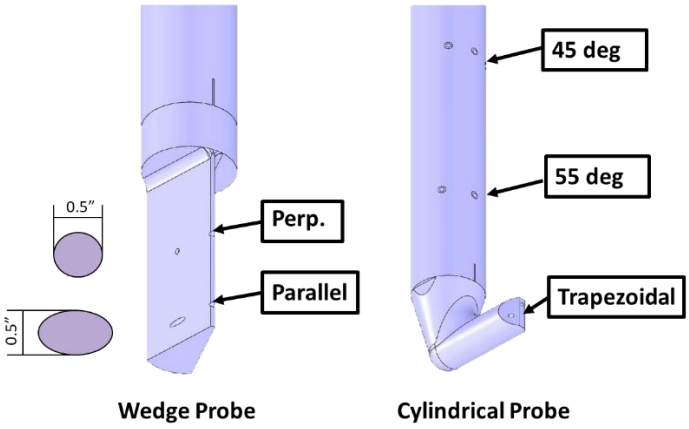

Figure 1. Experimental Yaw Probes (P1 And S3 Shown)
(Left) Wedge Probe type. The top and bottom rows of holes are perpendicular and parallel respectively.
(Right) Cylindrical Probe type. The top, middle, and bottom rows are 45°, 55°, and trapezoidal head respectively.

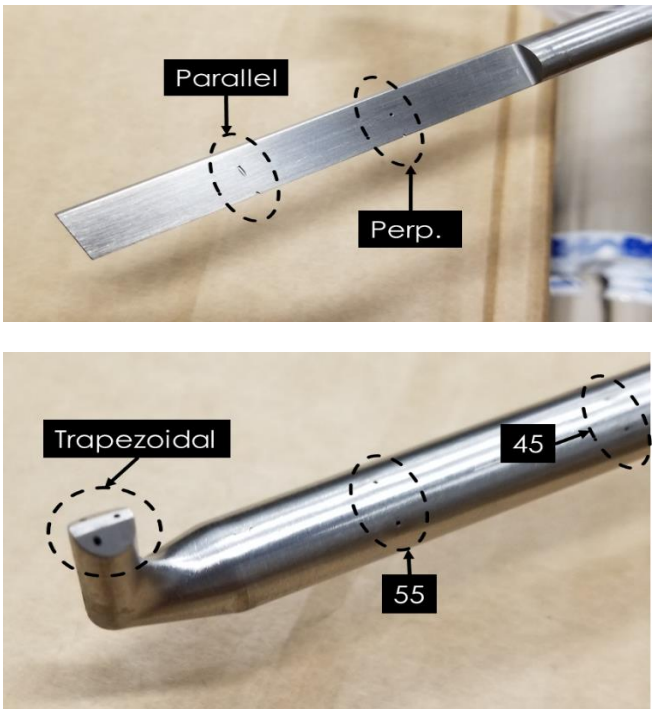

Figure 2. Yaw Probes Actual
(Top) 30° Wedge Probe (Bottom) Cylindrical Probe

Table 1. Experimental Test Probes

Probe type	Hole Configuration	Probe Head Angle
Wedge Probe	Parallel	Inclined Angle: 30 deg
	Perpendicular	Inclined Angle: 30 deg
Cylindrical Probe	Cyl 45	Radial Position ±45 deg
	Cyl 55	Radial Position ±55 deg
	Trapezoidal 45	Inclined Angle: 45 deg

Performance Drift from Sand Fouling

Microscopic images of each probe hole are captured before any particulate fouling tests. Each probe is calibrated, over a range of flow angles, in an open air jet to establish calibration curves from pressure measurements. These probes are calibrated over different flow angles to better understand the impact of flow direction on a partially blocked probe. The probes are calibrated under 2 Mach numbers to better understand the impact of increasing flow velocity on a partially blocked probe.

Once the clean probe's performance is documented and microscopic images taken of the hole geometry, the probe is fouled in a hot sand "Dirty Rig". Once fouled, microscopic images of the probe are taken again to track the amount of particulate deposited. The probe is then re-calibrated to determine the decline in performance from its initial baseline. This testing loop, is repeated until the probe is completely clogged, or it reaches the end of its testing space. In between each hot sand test, the sand on the probe is not cleared or removed.

EXPERIMENTAL TEST FACILITY

A. SUBSONIC AMBIENT TEMPERATURE OPEN AIR JET

For the purposes of calibrating the yaw probes, or recording pressure measurements of a range of flow angles, the probes are swept from [-40°:40°]. The effective range for 5-hole probes is ±30° [4], so the effective range of 3-hole probes is expected to be lower than ±30°.

Each probe is also calibrated at Mach numbers of 0.3 and 0.5. Realistic jet combustion chambers have Mach number flows of 0.3-0.4, with Mach 0.5 flows at the fuel injectors[5,6].

Equipment and Hardware

The Virginia Tech Calibration Jet, shown in Figure 3, is a subsonic, open air jet. It is operated exclusively at ambient temperatures. It is composed of a 36" long, 4" dia, and 304 stainless steel plenum with a 2" diameter subsonic contraction nozzle. A 2" diameter stainless steel flexible hose connects the plenum to shop air. The shop air is supplied at 175 psi, but passes through a regulator before reaching the plenum. The regulator allows for precise control of the exit Mach number from the nozzle. The process for calculating Mach number is described in detail in the following section.

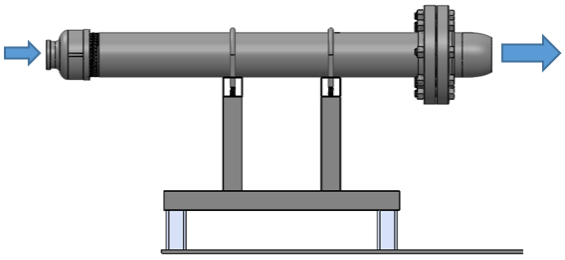

Figure 3. Virginia Tech Calibration Jet With 2" Dia Subsonic Contraction Exit Nozzle. Rotary Table and Device Not Shown.

Data Acquisition

The data acquisition setup consists of a Pitot-static probe, a pressure scanner, multiple pressure transducers, and a National Instruments Data Acquisition system (NIdaq). The pressure scanner, a 0-50 psi Zoc17 module, is capable of measuring up to 8 simultaneous pressure inputs within an accuracy of ±0.04 psi [7]. The Pitot-static probe connects to the pressure scanner to measure the stagnation and static pressures of the air within the plenum. The pressure transducers measure the pressure from the experimental yaw probes, and connect to the yaw probes through 1mm dia clear silicate tubing. These transducers are 0-5 psi and 0-10 psi Keller Valueline pressure transducers with accuracies of ±0.013 psi and ±0.025 psi respectively [8]. The pressure transducers and pressure scanner connect to a Pixie-NIdaq system, which uses LabVIEW to display and record measurements.

A Velmex rotary dial and Velmex motor controller make up the traverse assembly of the Calibration Jet. The traverse assembly, is used to actuate the experimental yaw probes over a set range of flow angles to develop calibration curves for each probe hole configuration. COSMOS, a software provided by Velmex, interfaces the motor controller to a computer. This allows for precise rotary control from within a separate control room. The accuracy of the setup, as defined by the Velmex datasheet [9], is ±0.08° with a rotational velocity of 2000 steps/sec at 20 steps/deg.

Calculating Mach Number

The pitot-static probe is used to measure the total pressure and static pressure of the stagnant air within the plenum. Plenum total pressure is used to calculate the expected Mach number of the flow exiting the jet. Plenum total pressure is also a reference pressure used to normalize pressure readings from the yaw probes. Exit Mach number is calculated using the compressible flow equation shown below:

$$\frac{P_T+P_S}{P_S} = \left(1+\frac{\gamma-1}{2}M^2\right)^{-\frac{\gamma}{\gamma-1}} \quad [1]$$

$$M = \sqrt{\frac{\gamma-1}{2}\left(\left(\frac{P_T+P_S}{P_S}\right)^{-\frac{\gamma-1}{\gamma}}-1\right)} \quad [2]$$

Where P_T is the plenum total pressure in gauge pressure, P_S is the static pressure in the room as determined by pressure readings measured from the local Blacksburg airport(adjusted for elevation), and γ is the specific heat ratio of dry air at room temperature(γ =1.4).

Assumptions include a calorically perfect gas, negligible wall friction, isentropic flow, and irrotational flow. The isentropic assumption works well for the majority of nozzles encountered in operation, with issues occurring when the nozzle is significantly small. If the nozzle and plenum diameters are greater than a few centimeters then the nozzle is much wider than the thickness of the boundary layer formed in the nozzle. This allows the flow to be treated as both isentropic and irrotational. In the previous equation, no inviscid assumption was made in order to accommodate the possibility of shock formation in the flow as described by Cantwell [10].

It is important to note that P_S is the static pressure in the room, not the static pressure within the plenum. Calculating Mach number using the static pressure in the plenum will result in a low Mach number measurement, since it would be calculating the Mach number within the plenum.

Jet Characterization

To characterize the free jet nozzle a 2-axis traverse system moved a pressure probe through a grid of measurement points both inside and outside of the flow. First, a single tube pressure probe was secured into the traverse and positioned 1" from the nozzle of the jet. Next, the pressure probe was connected to the Zoc17 pressure scanner. The jet was turned on and set to an intended exit Mach number of 0.3. Pressure data was recorded for 10 sec, every 0.16", over a 4"x4" grid around the nozzle. Figure 4 shows the results of this characterization. The standard error in Mach number was 0.1% over a sample area of 0.75" x 0.75".

Figure 4 shows that the jet has a uniform Mach number everywhere but around the edges, as expected. During testing each probe is placed around 1" from the jet exit, and near the center, so the probes will not experience significant differences in pressure from their position in front of the jet.

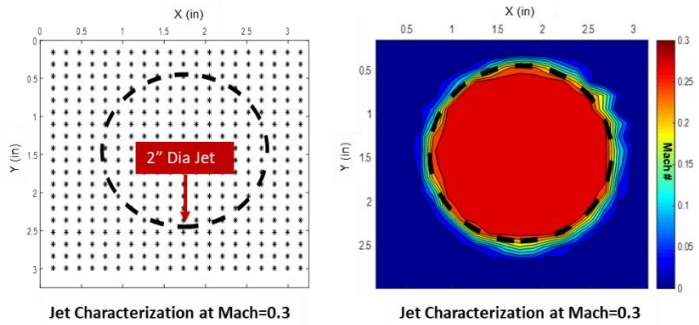

Figure 4. Mach Number Jet Characterization

A transient characterization of plenum pressure was also conducted to determine the variance in pressure at test conditions of Mach 0.3, and 0.5. Data was recorded at each measurement point for 10 seconds at a sampling rate of 100 Hz. These readings showed the error in measurement oscillated less than ± 0.013% FS for Mach 0.3 and ± 0.005% FS for Mach 0.5 setups. This accuracy is well within acceptable margins. The max error recorded from this experiment was about ± 0.004 Mach number for both Mach 0.3 and Mach 0.5. These were low in frequency and are negligible after time averaging. For a more detailed description of the analysis see Appendix A.

Nulled and Non-Nulled Modes

In order to calibrate 3-hole pressure probes, a "true zero" alignment was established. For this experiment, the probes are calibrated in a subsonic open-air jet. The 2 main accepted methods of calibrating pressure probes in an open air jet are Nulling mode and non-Nulled mode.

The Nulling mode involves seating a pressure probe in a multi-axis rotating actuator [11]. This actuator rotates the probe, while maintaining the tip in a relatively constant position [4, 12]. The zero angle is determined by rotating the probe until the static pressure holes on the sides of the probe read the same pressure [13]. This method requires a complicated traversing mechanism and can become very costly and time inefficient depending on the time constants of the probe itself.

The non-Nulled mode, also called the stationary method, involves seating a pressure probe in a rotating actuator as well. However, the rotation of the probe can be limited to just one axis of rotation, for example yaw angle, while pitch and roll angles are held constant with respect to the free jet. The stationary method, although less accurate, is much simpler and cheaper to implement. This simplicity makes it ideal for applications where space is limited for the traversing mechanism [13].

This experiment is conducted using a non-nulled mode. The pressure probes are secured within a yaw-only rotary traverse and rotated about the stem of the probe. The nozzle diameter is large relative to thickness of the probe. As such, all the probe holes are assumed as fully immersed in the flow from yaw angles of ± 40°.

Determining Zero Degree Flow Angle

For the purposes of this research, a "Zero Angle" is established relative to an exit jet flow of Mach 0.3. The probe is "zeroed" by pointing the probe into the flow and rotating the probe, in the yaw plane only, until the pressures from the static ports equalize. During this process the probe is moved in increments of 0.25° until the difference between the static pressure taps, labeled S2 and S3, reaches a minima, typically around ±0.005 psi. The position at this minimum is saved and recorded as the zero yaw angle. For the remainder of this report the process of determining zero yaw angle will be referred to as "zeroing the probe".

Note that zeroing the probe was performed at Mach 0.3 each time intentionally. Mach 0.5 flow carried further risk of flow separation across the static holes, which determine the zero angle. In the presence of flow separation, the difference between side holes would register a relatively unchanging value, even when changing yaw angle ~1-2°.

Probe Calibration Process

After zeroing the probes, the remainder of the calibration process begins. The probe is yawed throughout a predetermined range of yaw angles, shown in Table 2, and pressure data from the probe is recorded at each yaw angle. This process is repeated for Mach numbers of 0.3, and 0.5.

Table 2. Range Of Yaw Angles. Symmetric About Zero Such That There Are 21 Angles Total From [-40°:40°]

Yaw Angles	-40	-30	-25	-20	-15	-10	-8	-6	-4	-2	0

The probe is held stationary at each angle for a set amount of time, depending on the time constant for that particular probe, to ensure the readings have reached steady state. Preliminary shakedown testing showed that the probes reached steady state after a change in flow direction in <10s. During calibration, each probe was kept at a yaw angle for 20 seconds, before recording pressure data for an additional 10 seconds. The increased pause time was included to account for possible increases in time constants due to the probe holes being fouled

The probes used in this study are 3-hole per row yaw probes, which are only able to measure flow direction in the yaw plane. As such, the probes will be calibrated in the yaw plane only, the pitch and roll planes will be assumed constant since the probe will be firmly seated in a rotational actuator.

This research project will be introducing sand fouling onto the probes in a hot sand rig. As such the probe's hole geometry and surface roughness will change each test. In order to determine the effect of these changing parameters the probe is recalibrated in the ambient temperature jet after each sand fouling to develop a unique calibration curve relative to the degree of blockage the probe experiences.

B. VIRGINIA TECH AEROTHERMAL RIG (VTAR)

The Virginia Tech Aerothermal Rig(VTAR) is used for hot sand research and fouling studies. VTAR was donated by Rolls-Royce Indianapolis in 2010 and has been used for multiple particle deposition based research projects since it's arrival [14, 15, 16, 17]. Only slight modifications to the test section were required to facilitate probe-fouling experiments. A CAD rendering of the VTAR in "Probe-Fouling Configuration" is shown below in Figure 5. For a thorough description of VTAR operation, see Boulanger et al. [17].

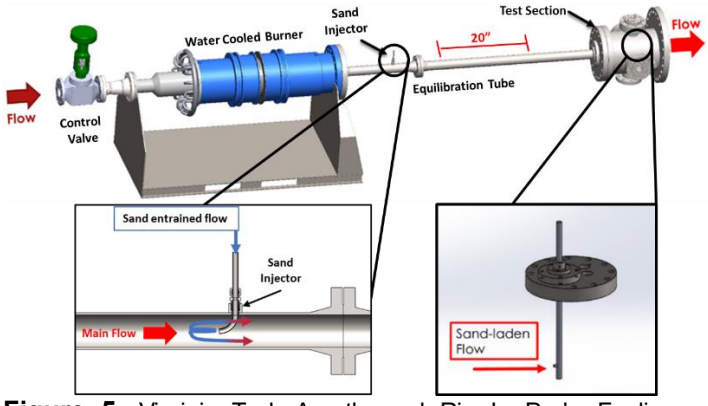

Figure 5. Virginia Tech Aerothermal Rig In Probe-Fouling Configuration

For this experiment, VTAR is operated at temperatures of 1050°C, atmospheric pressure of about 1 atm, and gas velocity of around 65 m/s. Two K-type thermocouples are secured with Inconel wire to the stem of the experimental probes while they are being tested. These thermocouples measure local flow temperature near the probe surface during hot operation.

Figure 6 shows thermocouple placement during a hot test. Once the local flow temperature stabilizes at 1050°C particulate injection is initiated via LabVIEW controls. After

sand fouling the probe is removed from VTAR and left to cool at ambient conditions.

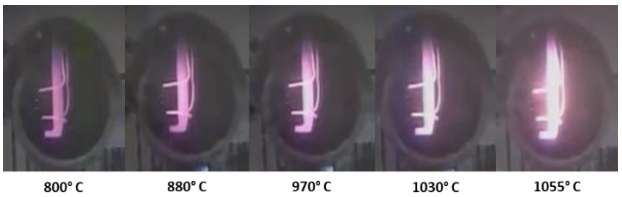

Figure 6. Cylindrical Probe Heated To 1050° C In Vtar Images Taken During Heat Up, Before Introducing ARD Into The System

Arizona Road Test Dust

The particulate for this report is 0-5 µm Arizona Road Dust (ARD). Arizona Road Dust is an ISO standard particulate that is widely used in turbomachinery research. Dunn et al. [2] found that the particulate that enters the hot section turbine area had a mean diameter of 6 µm. Bowen et al [18] developed a sticking efficiency model with 0-5 µm ARD able to anticipate particle impacts causing adhesion to the impacting surface. This model suggests that for the current operating temperature, 1050°C, nearly all particles below 6 um in diameter will stick to the surface of the probe. Boulanger et al.[16] experimented with melting points of 20-40 µm ARD and discovered the sintering point was around 1100°C for ARD particles less than 63 µm in diameter. 0-5 µm ARD at 1050°C is a good representative of the superheated sand particulate experienced in a real engine. At these temperatures the ARD is in a softened state and will adhere to the probe surface.

The ARD is injected over a 2 minute timeframe, which when well mixed correlates to a particular Parts per Million by Weight (PPMW) of sand to interact with the probe. Moisture is removed by baking the sand in a lab oven at 120°C for at least 36 hours prior to testing. Particles of 0-5 um ARD are so small that agglomeration rapidly occurs if even the slightest moisture is in it. For more information on 0-5 µm ARD please see the safety data sheet provided by Powder Technologies [19].

Sand loadings for the Wedge and Cylindrical hot tests are shown in Table 3 and Table 4 respectively. These loadings were chosen experimentally to develop a range of blockages with which to test the probe performance. For a thorough breakdown of ARD please see Appendix B

Table 3. Wedge Probe: Concentration Of ARD During Hot Sand Fouling

Test	Initial	Test 1	Test2	Test 3	Test 4	Test 5	Test 6
Sand Loading (g)	-	3	4	2	3	3	4
Sand Concentration (PPMW)	-	783	932	487	719	810	994

Table 4. Cylindrical Probe: Concentration Of ARD During Hot Sand Fouling

Test	Initial	Test 1	Test2	Test 3	Test 4	Test 5	Test 6
Sand Loading (g)	-	4	2	2	2	2	2
Sand Concentration (PPMW)	-	993.7	499.9	563	538.2	479.3	503.8

C. MICROSCOPIC IMAGING SETUP

Stereomicroscopy

Stereomicroscopes, often referred to as dissecting microscopes, are a unique type of binocular microscope capable of viewing high quality images of 3-dimensional objects[[20], [21]]. Traditional compound microscopes are more powerful than stereomicroscopes, but can only effectively focus on flat, or 2-D images [20]. This limitation restricts the use of compound microscopes to purposes involving small and thin objects such as dissection slides. The stereomicroscope does not suffer from this limitation, making it uniquely suited for applications where adequate inspection of a specimen requires 3-D observations that show both depth and contrast. Probe hole imaging is one such application. When coupled with a high quality digital camera, the stereomicroscope can take detailed images of multiple geometries of probe holes.

The stereomicroscope used in this study operates at 45x magnification and is equipped with a trinocular port accessory and a digital camera. The trinocular port takes the light that is be split between the binocular ports and renders a single image from them [21]. A 9 MP camera is placed in the trinocular port to take images of the specimen. This camera is restricted to reproducing 2-D images; however, the detail and quality are high enough that 3-D contours and geometry can be identified from the pictures. Additional magnification is available to the eyepiece lens through the zoom lens system in a stereomicroscope. Modern stereomicroscopes contain a zoom lens system that utilizes three or more lenses simultaneously to keep the object in focus and allow for precise control of added magnification [21]. Figure 7 shows a sample microscope image.

The light source used to view a specimen through a has a large impact on the quality of the image. Stereomicroscopes do not require that light be transmitted through a specimen, so they are often used to view opaque objects [22]. However insufficient lighting will cause shadows that will distort the image to be captured [21]. This experiment used a 56 bulb LED ring light, to adequately illuminate the specimen.

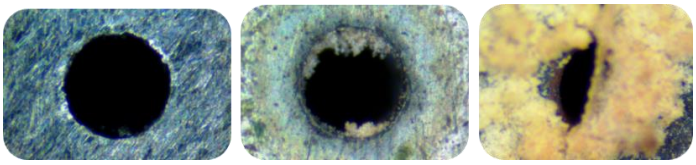

Figure 7. Cylindrical Probe P1 Images as Probe Becomes More Fouled. All Holes 0.51 Mm Dia.

RESULTS AND DISCUSSION

A. PROBE BLOCKAGE FROM SAND FOULING

Microscopic Imaging to determine Blockage

Microscopic imaging using the digital camera on the stereomicroscope produced high quality images of the sand buildup around the probe holes. Microscope images were taken after each sand test and again after each calibration test to record sand deposition and removal respectively. A 3-D printed probe holder was developed to make the size of the hole in the image uniform. In addition, the microscope was calibrated through a Calibration slide provided by the manufacturer AMSCOPE. Once the images of the probes were collected, an open source image processing software called FIJI [23] was utilized to measure the blockage in the probes.

Blockage Ratio Calculation

Clearance area and clean hole areas recorded from image analysis in FIJI were then used to calculate a non-dimensional Blockage Ratio (BLR) to relate probe hole sand blockage. The equation for BLR is shown below:

$$BLR = 1 - \frac{A_{clear}}{A_{clean}} \quad (3)$$

where, BLR is blockage ratio for a pressure hole, A_{clear} is the frontal area fluid can freely flow into the probe hole in pix^2, and A_{clean} is the frontal area of the probe hole initially in pix^2. Figure 8 shows the FIJI interface. The Clean and Clearance Areas are determined by tracing around the hole and sand blockage within the FIJI graphical user interface.

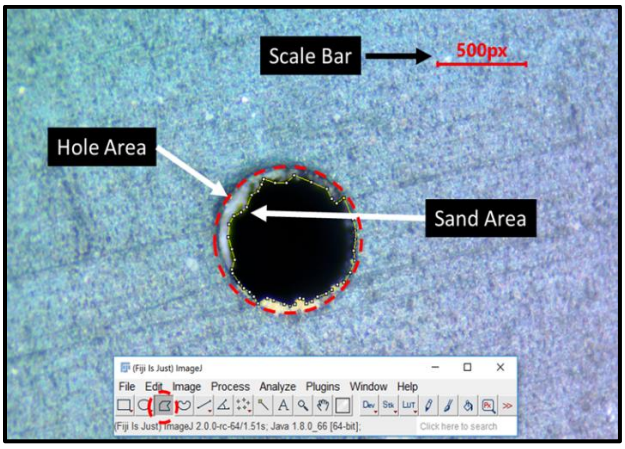

Figure 8. Image of Sanded Probe Hole in FIJI Interface

Probe Blockage from Sand Fouling

The corresponding BLR from hot testing is shown in Figure 9-Figure 13. These plots show test number on the x-axis. The whole number values on the x axis(1,2,3…) represent BLR after fouling while the half numbers(1.5,2.5,3.5…) represent BLR after calibration. The trends follow expectation, sand fouling increases the BLR of the probes while calibration reduces the BLR of the probes. For complete data set Blockage Ratios see Appendix E.

Wedge Probe Blockage

For Wedge configurations, the P1 center hole is expected to clog the fastest since it is impacted most directly by the sand flow and is the hottest point on the probe. The static ports, S2 and S3, experience a diverted sand flow and are expected to clog more slowly than the P1 hole. For both Wedge configurations the center hole clogged the most and the fastest.

The parallel configuration had surprisingly low BLR. This is due to the oblong shape the parallel static holes and a limitation in our microscope. Sand would be more likely to flow into the hole directly, and microscope images show that the deposition in these types of holes was almost exclusively at the trailing edge of the holes. It is suspected that there is more sand inside the hole itself, and is not entirely reflected by a surface analysis. As such, the low BLR of the parallel static holes should not be interpreted as a design strength, it is likely a weakness that equipment limitations cannot show adequately.

The perpendicular holes show expected trends, with the center hole getting the most blockage, and the side holes becoming more clogging as they are exposed to the sand longer. Note, Test 1 did not reach temperatures and no sand deposited on the probes. As such Test 1 is treated as initial, which is why the wedge graphs appear to only have 5 tests. Test #1 on the x-axis corresponds to Test 2 sand loadings.

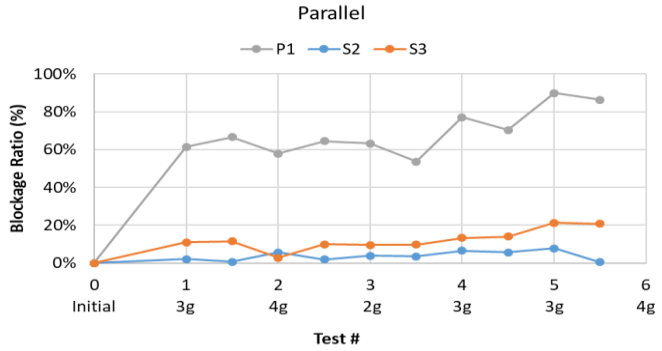

Figure 9. Narrow Wedge Parallel Blockage Ratio

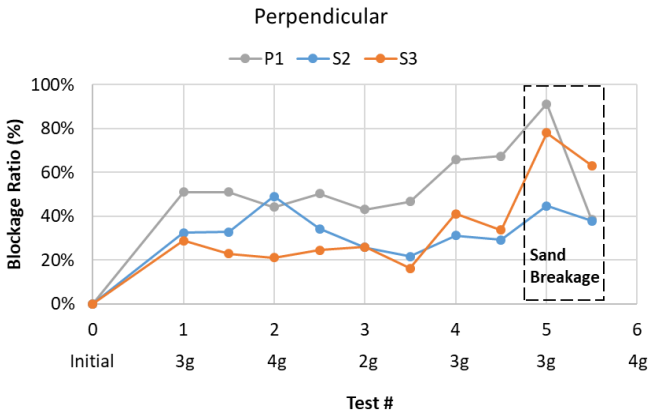

Figure 10. Narrow Wedge Perpendicular Blockage Ratio

Cylindrical Probe Blockage

For Cylindrical configurations, shown in Figure 11 and Figure 12, the P1 center hole is expected to clog the fastest since it is impacted most directly by the sand flow and is the hottest point on the probe. The static ports, S2 and S3, are expected to clog similar to the P1 hole in the absence of flow separation. A likely assumption with the relatively low velocity inside of VTAR. For both CYl 45° and Cyl 55° the center hole clogged the most and the fastest. Cyl 55° has consistently lower BLR, however this should not be interpreted as a design strength. The CYL 55° configuration was located 1" above and below the Trapezoidal and Cyl 45° probe. The jet itself is 2" in diameter, so during calibration this probe is exposed to the jet longer than the other two probes. The BLR of this probe is likely quite similar to that of the CYL 45°.

The Trapezoidal probe, shown in Figure 13, had a unique blocking trend. This was the only probe where the static holes clogged faster than the center hole. The static ports, S2 and S3, clogged significantly faster than the center port. The drastic reduction in BLR at Test 3.5 will be discussed in the next subsection.

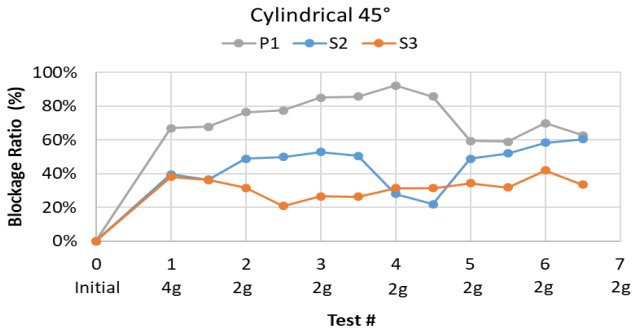

Figure 11. Cylindrical 45° Blockage Ratio

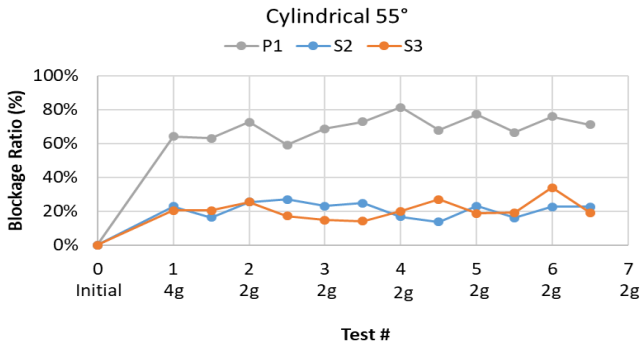

Figure 12. Cylindrical 55° Blockage Ratio

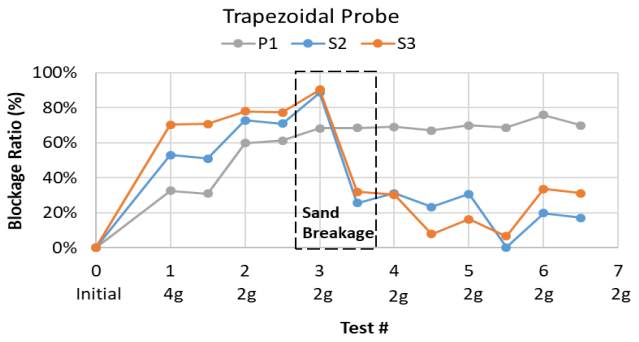

Figure 13. Cylindrical Trapezoidal Blockage Ratio

Sand Removal from Calibration: Thin Film Blockage

An interesting phenomenon noticed was sand being ripped off in chunks during calibration. This is seen most clearly by looking at the NW Perpendicular configuration and the Trapezoidal configuration shown in Figure 10 and Figure 13 respectively. For both configuration the probe was fouled to a BLR > 90%. The following calibrations resulted in large chunks of sand being removed, which dropped the BLR to >40%. This occurred in the P1 hole for the Wedge and both the S2 and S3 holes simultaneously for the Trapezoidal.

One hypothesis for his is significant reduction in blockage is explored here. The blockage over the probe holes appears to be a thin film of sand, as opposed to a thick agglomeration of sand. A pressure probe operates by reading the pressure of a stagnant column of air through a transducer. This air column creates a small pocket of pressurized air just inside the hole. Sand accumulates around this air pocket, unless the particles have enough kinetic energy to punch through it. This results in a thin film of glassified sand deposition over the hole. The surface area of this film increases until there is enough force from the calibration jet pressure to break it. Images after calibration show jagged residue on the perimeter of the holes after breakage, which supports this theory.

A temptation would be to consider this a design strength as well, but caution must be placed on making the assumption that the sand would break off the same way in an engine. During operation, temperatures stay hot as the air is flowing past the probes, so the blockage might not break away so easily. However, the process of thermally cycling the engine to clear debris might be helpful for the health of these measurement probes if it dislodged sand in the same manner.

Sand Removal during Hot-Test Cool down: Sand Peeling

During the hot sand procedure, the probes are removed from VTAR once they cool to <100°C and left to cool down in room temp air for 15-20 minutes. When the probes are first removed from VTAR there is a thin film of sand on the front face of the probe, in the case of the cylindrical probe, and the blade of the wedge, in the case of the wedge probe. This sand film peels off by itself as the probe cools down. This is due to a difference in thermal expansion between the sand and the metal. As the two dissimilar materials cool they contract at different rates causing the sand to separate from the metal surface. This implies that 1050°C is not sufficiently hot enough bond the ARD to the metal surface. This is a significant finding because it implies the sand deposits might peel off naturally from hot section probe hardware during downtime.

The remaining sand in the holes is measured using the previously described microscope technique. For safety concerns the probes were not placed under the microscope until they had fully cooled. As such the BLR data corresponds to the blockage in the probes after they have been cool, and the films of sand peeled off.

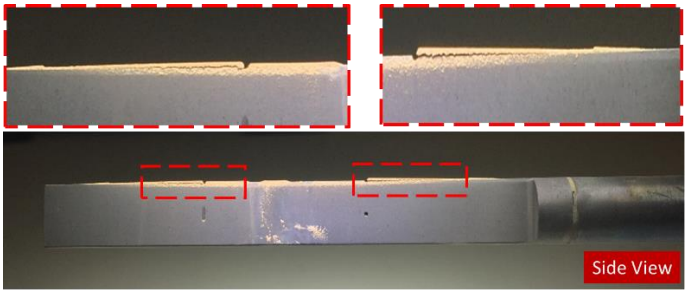

Figure 14. Sand Peeling on a Wedge Style Probe

B. PRESSURE MEASUREMENTS

Calibration pressure data is used to calculate dimensionless pressure coefficients. These pressure coefficients, when plotted versus the flow direction they were measured at, represent a calibration curve of that probe. This calibration curve can then be applied to pressure data from the yaw probes to calculate a flow direction anywhere over the same range of yaw angles for the same probe geometry. Note that calibration curves are only valid for the conditions they are tested at [4]. It is recommended that probes be calibrated individually to develop unique calibration curves. Minute manufacturing differences will affect calibrations slightly [13].

Dimensionless Pressure Coefficients

Pressure data from aero-calibration is used to calculate Yaw, Total, and Stagnation pressure coefficients using the following equations:

$$C_{yaw} = \frac{P_2 - P_3}{P_t - P_s} \quad (4)$$

Where C_{yaw} is dimensionless Yaw Coefficient.

Figure 20-Figure 24 show the calibration curves for the experimental yaw probes. Regions that appear relatively flat w.r.t the Yaw Coefficient, or have slopes that are becoming relatively flat, are not useful for the purposes of determining flow direction. In regions where the slope approaches zero the probe no longer responds to changes in flow angle. This can be due to many factors, the dominant factor being the hole is removed from the flow, or there is flow separation. Sand fouling has an impact on the probe's performance, so effect ranges of flow angles will be assessed based on the initial calibration data for each probe. Please note, the ranges of effective flow angles described in this report are based on data recorded at predetermined flow angles in increments of 5°. A more precise measurement is required to determine a universal range of angles for each probe.

The effect of the changes in the calibration curve from sand fouling will be explored in detail in the following section.

Initial Calibration Curves

Each probe was calibrated in the ambient temperature calibration jet before any sand fouling was conducted. The results from the initial calibrations for each probe, in terms of C_{yaw}, are shown below in Figure 15- Figure 19. An effective range of angles is determined to be the range of angles over which there is continuously increasing or decreasing slope of the C_{yaw} vs Yaw angle graph. This means that changing yaw angle has a significant effect on the probe measurements.

The parallel holes had an unexpected effective range of angles. There was an increasing slope between ±20° for Mach 0.3 and ±15 for Mach0.5. However, the graph went slightly flat for angles near 0°, implying that this probe configuration is not good for measuring small flow angles, or for measuring larger flow angles. For the Perpendicular wedge configurations, the effective ranges are between ±20° for Mach 0.3, and ±15° for Mach 0.5. However, the slope of the graph decreases significantly for Mach 0.5 outside the [-15°:15°] of yaw

For CYL 45° the effective range is ±20° at Mach 0.3, and ±15 at Mach 0.5. For CYL 55° the effective range is ±20° at Mach 0.3, and ±10° at Mach 0.5. However, the slope approaches 0 over at flow angles between [-2°:2°] at Mach 0.5. The Cylindrical 55° probe, for the Mach 0.5 case, had a slope close to zero for small angles < ±4°, the Cyl 55° is not well suited for flow directional measurement. For both Cylindrical probes increasing the Mach number increased the slope of the yaw coefficient graphs for larger flow angles. Increasing the Mach number also made the slope of the yaw coefficient graph more irregular for smaller flow angles. The Trapezoidal probe had the largest effective range of ±30° at Mach 0.3, and ±25° at Mach 0.5.

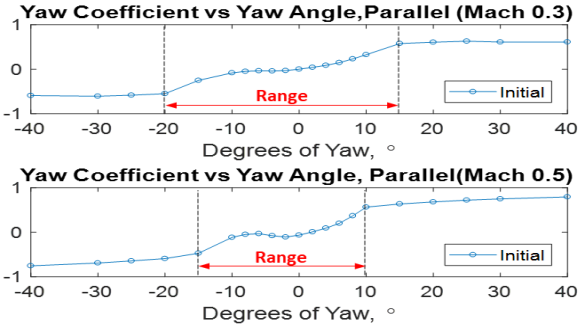

Figure 15. Wedge Parallel Yaw Coefficients over [-40°:40°] range of flow direction (Initial Calibrations Only)

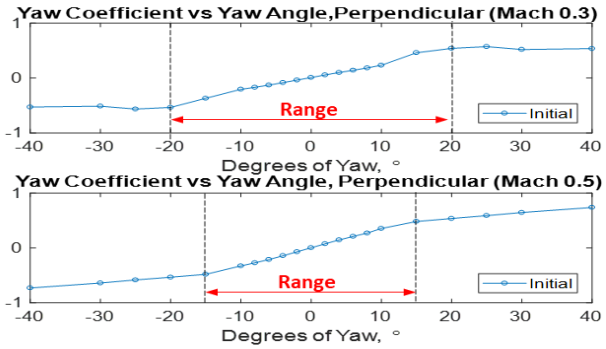

Figure 16. Wedge Parallel Yaw Coefficients Over [-40°:40°] Range Of Flow Direction (Initial Calibrations Only)

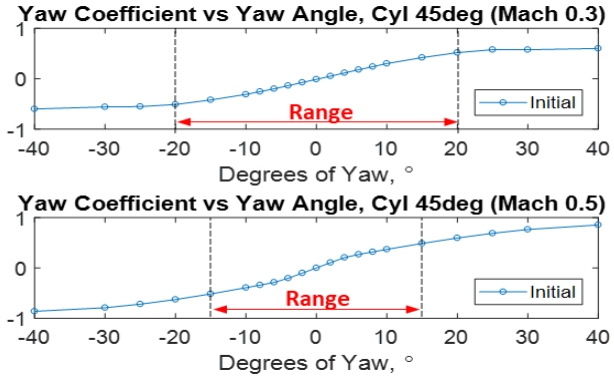

Figure 17. Cylindrical 45° Yaw Coefficients Over [-40°:40°] Range Of Flow Direction (Initial Calibrations Only)

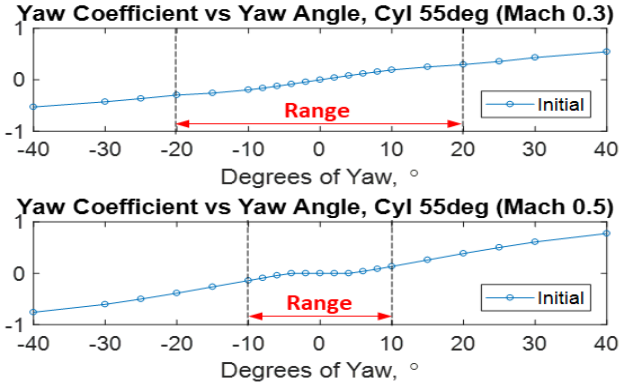

Figure 18. Cylindrical 55° Yaw Coefficients Over [-40°:40°] Range Of Flow Direction (Initial Calibrations Only)

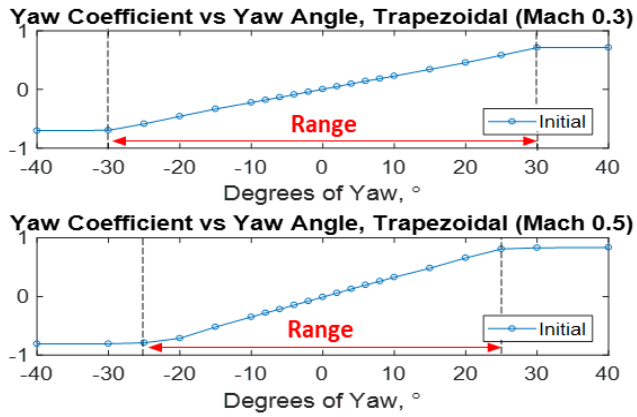

Figure 19. Trapezoidal Yaw Coefficients Over [-40°:40°] Range Of Flow Direction (Initial Calibrations Only)

Wedge Probe Calibration Curve

Figure 20 and Figure 21 show the yaw coefficients for the parallel and perpendicular wedge probe configurations over flow directions of -40°:40° of yaw. The parallel holes performed similarly after fouling, except at the higher Mach number. Mach 0.5 for the parallel holes had significant differences in performance from sand fouling. There was an increasing slope between ±20° for Mach 0.3 and ±15 for Mach0.5. However, the graph went slightly flat for angles near 0°, matching the trends seen in the initial calibration

For the Perpendicular wedge configurations, after fouling, the effective ranges are between ±20° for Mach 0.3, and ±15° for Mach 0.5.

The Parallel configuration has much more variance in readings than the Perpendicular configuration from the sand fouling. As mentioned previously the relatively lower BLR does not indicate a better performance for the Parallel probe.

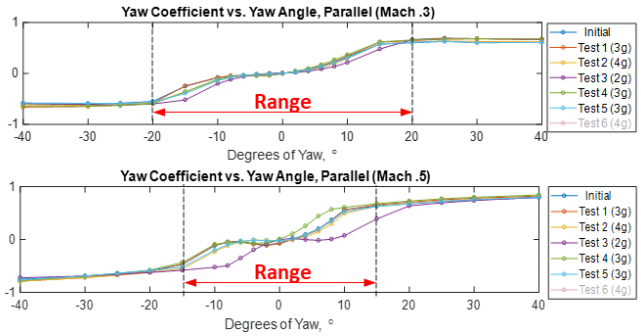

Figure 20. Narrow Wedge Parallel Yaw Coefficients Over [-40°:40°] Range Of Flow Direction. Test 6 Had A Significant Change In Yaw Coefficient And Was Removed For Clarity Of Results.

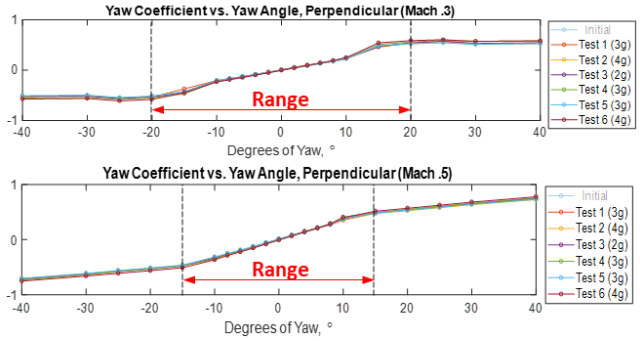

Figure 21: Narrow Wedge Perpendicular Yaw Coefficients Over [-40°:40°] Range Of Flow Direction. Error During Initial Calibration. Test 1 Used As Initial

Cylindrical Probe Calibration Curve

Figure 22 and Figure 23 show the yaw coefficients, after sand fouling, for the CYL 45° and CYL 55° probes respectively. For CYL 45° the effective range is ±20° at Mach 0.3, and ±15 at Mach 0.5. For CYL 55° the effective range is ±20° at Mach 0.3, and ±10° at Mach 0.5. However, for the 55° probe, the slope approaches 0 over at flow angles between [-4°:4°] at Mach 0.5. This probe is not well suited for flow directional measurement, and will experienced increased error in flow direction measurement. In addition, the initial calibration curve and the fouled calibration curves for CYL 55° were significantly different in slope and behavior. The initial calibration was done twice for repeatability. This led to the conclusion that the sand fouling significantly changes the performance of this probe configuration. Large errors in yaw angle measurement are expected for this probe. For both Cylindrical type probes the sand fouling appears to slightly improve the useful ranges of the yaw coefficient. The effects of changing surface roughness on the pressure distribution and flow separation mechanics on a cylindrical probe are well documented [24, 25, 26]. Even slight changes to surface roughness will affect the pressure distribution around the cylinder. In addition, increasing surface roughness has been shown to increase the Reynold's number of the flow, which in turn reduces flow separation around the rear of the cylinder.

Figure 24 shows the yaw coefficients for the Trapezoidal probe. This probe had the largest effective range at ±30° at Mach 0.3, and ±25° at Mach 0.5.

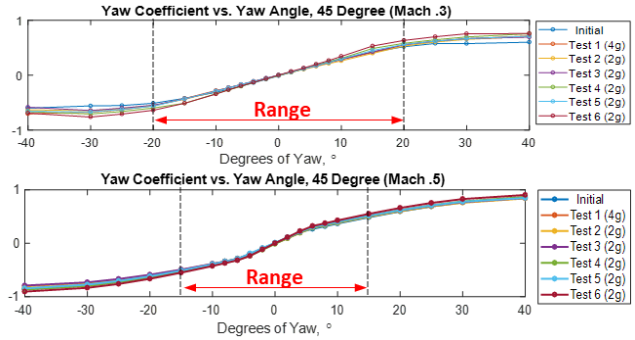

Figure 22. Cylindrical 45 Yaw Coefficients Over [-40°:40°] Range Of Flow Direction

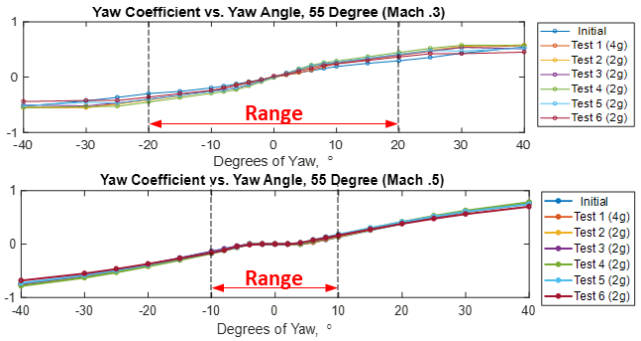

Figure 23. Cylindrical 55 Yaw Coefficients Over [-40°:40°] Range Of Flow Direction

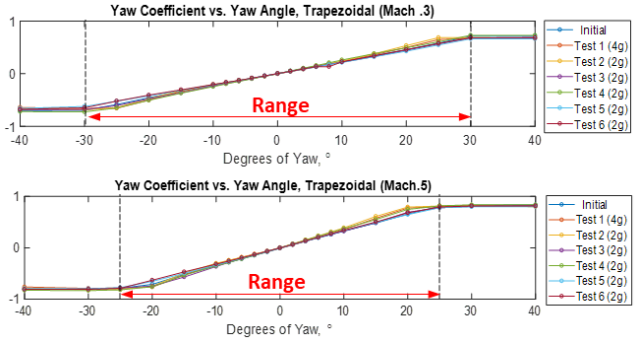

Figure 24. Cylindrical Cobra Yaw Coefficients Over [-40°:40°] Range Of Flow Direction

C. FLOW DIRECTION MEASUREMENT ERROR

Interpolation Functions

The Yaw Coefficient is used to calculate flow direction when compared to the calibration curve of a clean probe. A flow direction range of -20°:20° of yaw appeared to be a stable region for all probes, with the exception of the parallel head on the wedge probe. We decided to use this range to analyze the sensitivity of the probes to the sand fouling.

C_{yaw} data over the range of -20°:20° from each initial clean calibration is used to calculate a measured yaw angle from the fouled calibration data. The procedure for determining the error in yaw measurement is as follows:

1) Invert Coefficient plots so C_{yaw} is on the x-axis and flow direction on the y-axis.
2) Fit a cubic interpolation to the initial C_{yaw} data.
3) Input C_{yaw} data from testing into interpolation function to calculate a measured yaw angle, θ_{meas}.
4) Calculate Yaw Angle Measurement Sensitivity, δ_θ using the following equation:

$$\boldsymbol{\delta_\theta = |\theta_{act} - \theta_{meas}|} \quad (5)$$

where, θ_{act} is the flow direction the probe is seeing, θ_{meas} is the flow direction calculated from the yaw coefficient of a fouled probe.

Interpolation functions performed similarly to polynomial fit for most cases, but was much easier to implement. In addition, in regions where the C_{yaw} graph slope increased dramatically the polynomial fit created dramatic errors when attempting to interpolate values between data points. Sumner [0004] compared the error involved in using interpolation function and polynomial fit to interpolate between calibration points in a 7-hole pressure probe. He found that the interpolation functions performed better in the presence of flow separation. Coefficient data from probe hole showed trends that indicate flow separation in regions of dramatic slope changes of the C_{yaw} plots.

Flow Direction Measurement Sensitivity to Sand Fouling

In the following figures, yaw angle measurement sensitivity, δ_θ, is plotted vs flow angle. Equation 4 shows that only the S2, and S3 holes are needed from the yaw probe to calculate C_{yaw}. As such, the average BLR of the two will represent blockage that would affect the probe readings. During calibration the probes are zeroed based on the reading from the side holes. If one side was significantly blocked, while the other wasn't, the zero angle determined from the S2 and S3 holes would be offset. The misalignment of the zero angle would also offset the measurements at the remaining flow directions. This offset is treated as a physical response, since in operation the probes would likely be fixed in place, at a known angle. The difference in pressures from the blocked S2 and S3 holes would affect the pressure coefficients calculated from the pressures measured from those side holes.

δ_θ is plotted vs the average BLR between S2 and S3, as well as the P1 center hole BLR. Data analysis on the errors show that the average (S2,S3) BLR better describes the error trends in yaw angle measurement. Errors in Yaw angle measurement were slightly asymmetric for the probes, and those interested in determining an optimal range of angles need to consider how to best orient the probe to get the widest range of angles with the least error.

The NW Parallel and CYL 55° holes performed the worst out of the probe designs. The parallel due to the shape of the calibration curve and the effect of sand deposition. The 55° due to the sand fouling significantly altering the shape of the calibration curve of that probe.

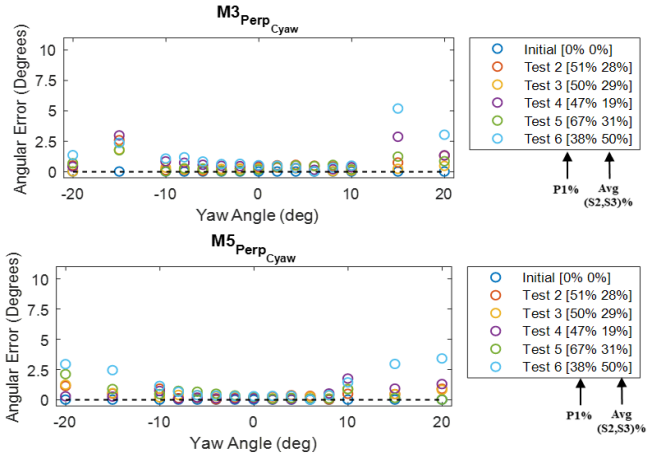

Figure 25. Narrow Wedge Perpendicular Yaw Angle Measurement Error Over A Range Of Flow Directions [-20°:20°]

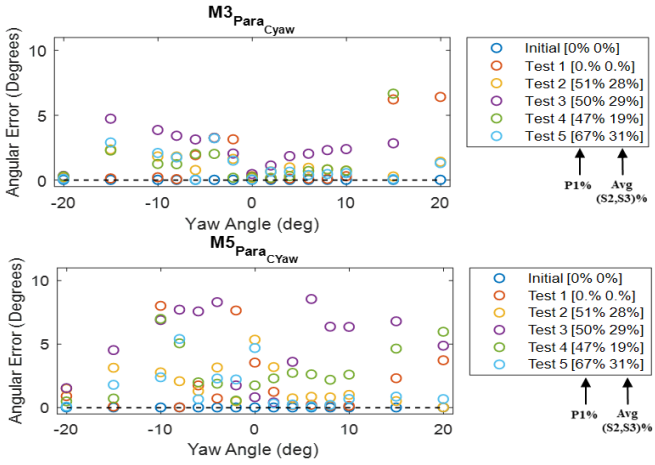

Figure 26. Narrow Wedge Parallel Yaw Angle Measurement Error Over A Range Of Flow Directions [-20°:20°]

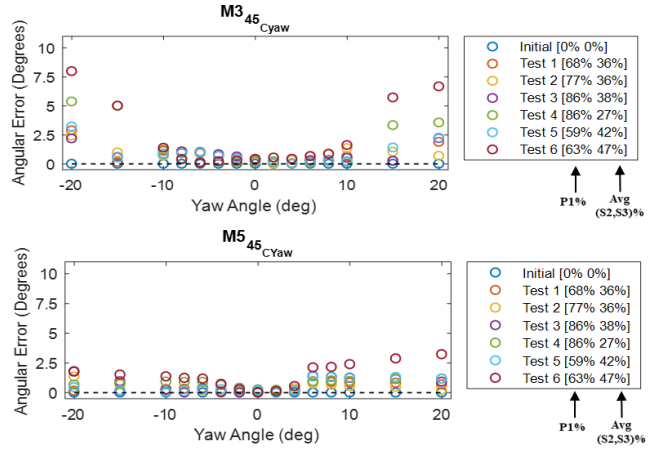

Figure 27. Cylindrical 45° Yaw Angle Measurement Error Over A Range Of Flow Directions [-20°:20°]

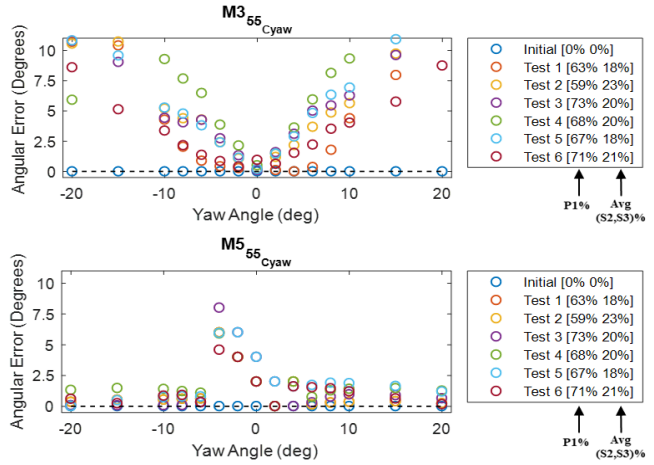

Figure 28. Cylindrical 55° Yaw Angle Measurement Error Over A Range Of Flow Directions [-20°:20°]

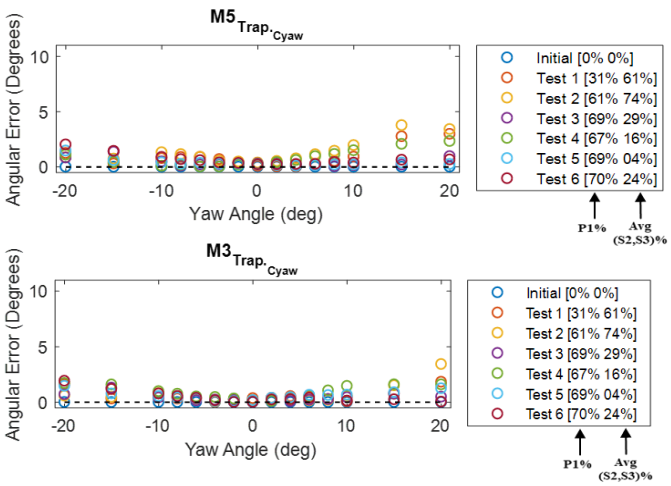

Figure 29. Cylindrical Trapezoidal Yaw Angle Measurement Error Over A Range Of Flow Directions [-20°:20°]

Max Flow Direction Error Over [-10°:10°]

The probes used in this study had escalating errors outside of the ±10° range. Table 5 shows these errors.

Table 5. Max Flow Direction Measurement Error from [-10°:10°]

30° Wedge Probe		Initial Error(deg)	AVG BLR(S2,S3)	Max Error CYAW (deg)
M=0.3	Parallel	1.0	11%	3.8
	Perp	0.1	51%	1.2
M=0.5	Parallel	2.5	11%	8.5
	Perp	0.1	51%	1.7
Cylindrical Probe		Initial Error(deg)	AVG BLR(S2,S3)	Max Error CYAW (deg)
M=0.3	45°	0.6	47%	1.6
	55°	0.2	22%	9.6
	Cobra	0.3	74%	1.5
M=0.5	45°	0.2	47%	2.4
	55°	8.0	22%	8.0
	Cobra	0.2	74%	2.0

Comparing Probes at a Similar BLR

In order to accurately compare the effects performance of the probes together the 3 best performing probes (Perp., Cyl 45, Trap.) were plotted over ±10°. The Perpendicular probe and Cylindrical 45 probe had similar max average side hole blockages of about 50%. The closest to this blockage was about 60% for the Trapezoidal Probe. Figure 30 shows the result of this study. The results are relatively symmetric, although not perfectly centered on zero, with a few differences that don't take away from the overall trends. These results matched expectations results. Error in the wedge probe wasn't sensitive to small changes in flow directions(~ ±4-6), while both the cylindrical and trapezoidal probes had error that highly parabolic with a minima around that probes zero angle [4]. The wedge probe appears to perform the best under similar conditions to the other two probes, despite being exposed to more sand during testing.

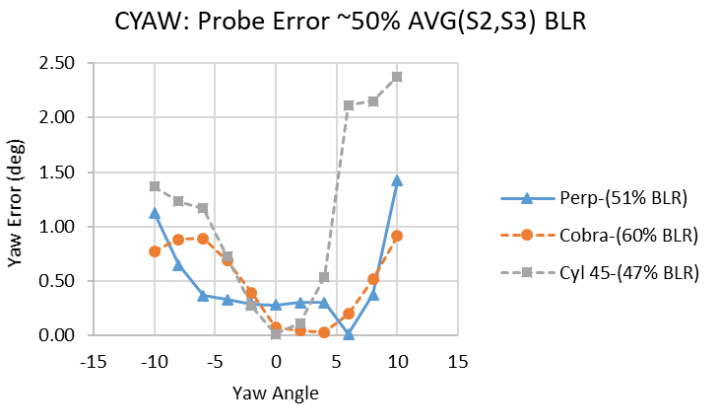

Figure 30. Flow Direction Measurement Error For A Similar Blockage Ratio, Over A Range of Flow Directions of -10 to 10 Deg.

SUMMARY AND CONCLUSION

The objective of this experiment was to develop a better understanding of the sensitivity of experimental 3-hole pressure probe designs to engine realistic sand fouling. The probes tested included 3 geometries: a wedge probe, a cylindrical probe, and a trapezoidal probe. All probes used were made of the same nickel super-alloy material. The wedge probe, a 30° wedge, had perpendicular and parallel sets of 3-hole probes built in. The cylindrical geometry, had 45° and 55° radial yaw probe configurations built into it. The last probe configuration was the trapezoidal probe. Each of these probes experienced accelerated sand testing in a realistic "Dirty Rig" environment in the Virginia Tech Aerothermal Rig. The probes were fouled by 0-5 µm Arizona Road Dust, heated to 1050°C at 65m/s, for a duration of 2 minutes each test. The probes were then calibrated after each hot test to determine the degradation in sensor measurements. Microscopic images were taken with a digital camera attached to a stereomicroscope to accurately quantify probe blockage. The data from all 3 experiments was compiled to develop graphs showing the effect of probe blockage due to sand fouling on flow direction measurement by the probes.

Sand was also removed due to natural sand peeling off of the experimental probes during cool down, immediately following hot sand testing. Significant deposits of sand was removed during the calibration process, which is indicative of the effects of cold start conditions in a realistic engine.

Accelerated erosion testing showed that the perpendicular wedge design had the least blockage in Static holes, even though the Wedge probe was fouled with the most sand. The trapezoidal probe clogged by far the fastest and was the only probe that clogged in it's static pressure ports before it's center hole. Further data analysis revealed that the average blockage between the two side holes, labeled S2 and S3, was more of a significant factor in determining probe error than the Blockage of the center, stagnation, hole.

In addition the wedge probe had lower flow directional measurement errors than the other probes for both Mach 0.3 and Mach 0.5. Over a range of flow directions from [-10°:10°] the Perpendicular wedge probe had flow direction measurement errors of 1.2° and 1.7° respectively. The 45° Cylindrical probe and Trapezoidal probes were comparable. The 45° Cylindrical probe had errors of 1.6° and 2.4°, respectively, from [-10°:10°] The trapezoidal probe had errors of 1.5° and 2.0° respectively, from [-10°:10°]. The Parallel Wedge and 55° Cylindrical probes performed much worse than the three previously mentioned.

REFERENCES

[1] Murugan, M., Ghoshal, A., Walock, M., Nieto, A., Bravo, L., Barnett, B., Pepi, M., Swab, J., Pegg, R. T., Rowe, C., Zhu, D., and Kerner, K., 2017, "Microstructure Based Material-Sand Particulate Interactions and Assessment of Coatings for High Temperature Turbine Blades," Volume 2D: Turbomachinery, p.1-2 V02DT48A009.

[2] Dunn, M.G., Padova,C.and Adams, R.M. Operation of Gas Turbine Engines in Dust-Laden Environments, ADP006197, 1987, Buffalo, New York, US.

[3] Owusu, Daniel & Pokhrel, Manish & Cho, J. (2016). CFD simulation study of de-icing on a pitot tube. International Journal of Applied Engineering Research. 11. 2986-2989.

[4] C. Tropea, *Springer handbook of experimental fluid mechanics: with DVD-ROM, 1240 figures and 123 tables*, vol. 1. Berlin: Springer, 2016.Pages: 228-229

[5] M. Gieras and T. Stańkowski, "Computational study of an aerodynamic flow through a micro-turbine engine combustor," *Journal of Power Technologies*, vol. 92, no. 2, pp. 68–74, 2012.

[6] O. Bodin, "Numerical Computations of Internal Combustion Engine related Transonic and Unsteady Flows," Royal Institute of Technology, Stockholm, Sweden, tech., 2009.https://www.diva-portal.org/smash/get/diva2:160394/FULLTEXT01.pdf

[7] "Model ZOC17 Temperature Compensated Electronic Pressure Scanning Module." Scanivalve Corp, Liberty Lake, 2014. http://scanivalve.com/media/27679/zoc17_1402.pdf

[8] "Keller Valueline High Accuracy Pressure Transmitter Datasheet PDF." Keller America Inc, Newport News. https://www.instrumart.com/assets/valueline-datasheet.pdf

[9] "Rotary Table Spec Overview." Velmex Inc, Bloomfield, NY.https://www.velmex.com/Downloads/Spec_Sheets/Rotary Tables Spec Overview.pdf

[10] Cantwell, Brian. "AA210A Fundamentals of Compressible Flow: Chapter 10 Gasdynamics of Nozzle Flow." Standford University, Aug. 2017. https://web.stanford.edu/~cantwell/AA210A_Course_Material/AA210A_Course_Notes/AA210_Fundamentals_of_Compressible_Flow_Ch_10_BJ_Cantwell.pdf

[11] H. Hodson, "pressure-probes," *Teach Yourself Phase Diagrams*. [Online]. Available: http://www-g.eng.cam.ac.uk/whittle/current-research/hph/pressure-probes/pressure-probes.html. [Accessed: 05-May-2018].

[12] T. J. Dudzinski and L. N. Krause, “Flow direction measurement with fixed-position probes,” Nasa Lewis Research Center, Cleveland, OH, tech., 1969.https://ntrs.nasa.gov/archive/nasa/casi.ntrs.nasa.gov/19690030674.pdf

[13] D. L. DÍAZ, “Experimental Calibration of Three-Hole Pressure Probes with Different Head Geometries ,” thesis, 0AD.

[14] Boulanger A, Patel H, Hutchinson J, et al. Preliminary Experimental Investigation of Initial Onset of Sand Deposition in the Turbine Section of Gas Turbines. ASME. Turbo Expo: Power for Land, Sea, and Air, Volume 1: Aircraft Engine; Fans and Blowers; Marine ():V001T01A003. doi:10.1115/GT2016-56059.

[15] Barker B, Hsu K, Varney B, Boulanger A, Hutchinson J, Ng WF. An Experiment-Based Sticking Model for Heated Sand. ASME. Turbo Expo: Power for Land, Sea, and Air, Volume 2D: Turbomachinery ():V02DT48A014. doi:10.1115/GT2017-64421.

[16] Boulanger, A., Hutchinson, J., Ng, W. F., Ekkad, S. V., Keefe, M. J., Xu, W., Barker, B., and Hsu, K., 2017, “Experimental investigation of the onset of sand deposits on Hastelloy-X between 1,000°C and 1,100°C,” The Aeronautical Journal, **121**(1242), pp. 1187–1199.

[17] Boulanger A, Hutchinson J, Ng WF, et al. Experimental Based Empirical Model of the Initial Onset of Sand Deposits on Hastelloy-X From 1000°C to 1100°C Using Particle Tracking. ASME. Turbo Expo: Power for Land, Sea, and Air, Volume 2D: Turbomachinery ():V02DT48A015. doi:10.1115/GT2017-64480.

[18] Bowen, C. P., Libertowski, N. D., and Bons, J. P., 2018, “Modeling Deposition in Turbine Cooling Passages With Temperature,” pp. 1–15.
[0004] D. Sumner, “A Comparison of Data-Reduction Methods for a Seven-Hole Probe,” *Journal of Fluids Engineering*, vol. 124, no. 2, pp. 523–527, 2002.

[19] K, Lux E. “Arizona Test Dust (ATD) Safety Data Sheet.” Powdertechnologyinc.com, 4 Feb. 2016. http://www.powdertechnologyinc.com/wp-content/uploads/2012/08/SDS.01.Arizona-Test-Dust.4-Feb-2016-1.pdf

[20] “HOW TO CHOOSE A MICROSCOPE,” Microscope Parts and Functions. [Online]. Available: https://www.amscope.com/how-to-choose-microscope. [Accessed: 20-Jun-2018].

[21] P. E. Nothnagle, W. Chambers, and M. W. Davidson, “Introduction to Stereomicroscopy,” Nikon's MicroscopyU. [Online]. https://www.microscopyu.com/techniques/stereomicroscopy/introduction-to-stereomicroscopy. [Accessed: 20-Jun-2018].

[22] “Stereo Microscopes,” *10 Fun Facts about the History of the Microscope*. [Online]. Available: https://www.microscopeworld.com/c-429-stereo-microscopes.aspx. [Accessed: 20-Jun-2018].

[23] Schindelin, J.; Arganda-Carreras, I. & Frise, E. et al. (2012), "Fiji: an open-source platform for biological-image analysis", *Nature methods* **9(7)**: 676-682, PMID 22743772, doi:10.1038/nmeth.2019 (on Google Scholar).

[24] O. Güven, C. Farell, and V. C. Patel, “Surface-roughness effects on the mean flow past circular cylinders,” Journal of Fluid Mechanics, vol. 98, no. 04, p. 673, 1980.

[25] Duarte Ribeiro, JoséLuis. (1991). Effects of surface roughness on the two-dimensional flow past circular cylinders I: mean forces and pressures. Journal of Wind Engineering and Industrial Aerodynamics. 37. 299-309. 10.1016/0167-6105(91)90014-N.

[26] Davenport, W.J. (2003), “Flow Past a Circular Cylinder”, Virginia Tech University. Online. Internet. 9 Oct. 2003. Available: www.aoe.vt.edu

[0024] T. J. Dudzinski and L. N. Krause, “Flow-direction measurement with fixed-position probes,” NASA Lewis Research Center, Cleveland, OH, tech., 1969.

[0025] R. L. raves, “Effect of Pressure and Turbine Inlet Temperature on the Efficiency of Pressurized Fluidized Bed Power Plants,” Volume 1B: General, vol. 80, no. GT, Oct. 1980.

[0026] K. Kano, H. Matsuzaki, K. Aoyama, S. Aoki, and S. Mandai, “Development Study of 1500°C Class High Temperature Gas Turbine,” Volume 4: Heat Transfer; Electric Power; Industrial and Cogeneration, Mar. 1991.

ATTRIBUTIONS

Several colleagues aided in the writing, researching, experimentation, and data analysis of this project.

Matthew Bogdan assisted in every aspect of this research project. Daniel VanHout assisted and conducted several experiments, analyzed data, invented innovative solutions, and assisted in active research efforts to improve processes. Smriti Kandel collected and analyzed data, assisted in laboratory experimentation, mentored new teammates and developed data packages. Kavi Muraleetheran had an integral role in developing analysis tools, and was responsible for many of the critical codes used in this research. Ansh Kapoor assisted in experimentations, and the rest of the team played integral roles in the success of this research project.

Andrew Boulanger laid the foundation for the VTAR approach used in this project. Vy Nguyen offered assistance and guidance, especially when hardware faced difficulties.

APPENDIX A. CALIBRATION JET

Calibration Jet Pressures Variation:

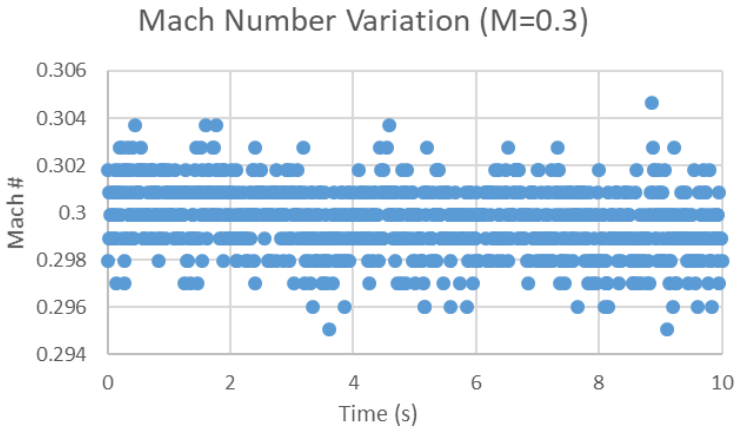

Figure 31. Mach Number Variation In Calibration Jet For Mach 0.3 Operation

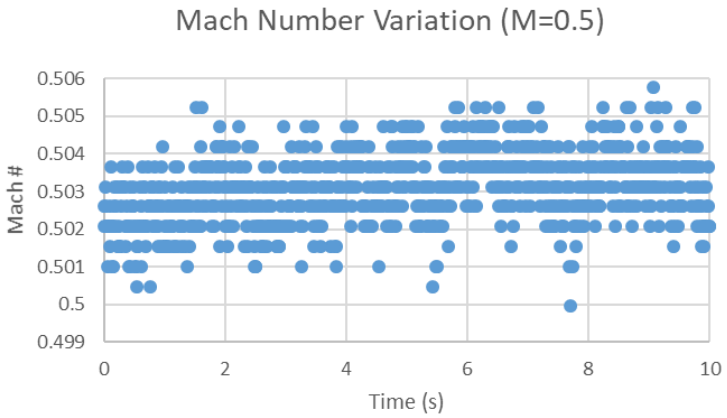

Figure 32. Mach Number Variation In Calibration Jet For Mach 0.5 Operation

Equations A1-A4 were utilized to analyze the Mach number data from the Calibration jet.

$$\bar{x} = \frac{\sum x_i}{n} \qquad [A1]$$

$$s = STD.s = \frac{\sum_{i=1}^{n}(x_i - \bar{x})^2}{n-1} \qquad [A1]$$

$$\epsilon = \left(\frac{(\bar{x}+s_x)-\bar{x}}{\bar{x}}\right) \cdot 100\% \qquad [A3]$$

$$s_x = \frac{s}{\sqrt{n}} \qquad [A4]$$

Where, s is the sample standard deviation in Mach number readings, s_x is the sample mean standard deviation from target Mach number, ϵ is the percent error from target Mach number, x is the value associated with integer j, xbar is the sample mean, and n is the total number of data points in the set, or in x, must be a positive integer. The results from these equations is shown below in Table 6.

Table 6. Calculated %Error And Standard Deviation Of Exit Mach# In Calibration Jet During Operation

	Standard Error			
	Std Dev S	Mean	STD Mean S_x	%Error
M=0.3	0.0014	0.300	3.92E-05	0.013
M=0.5	0.0009	0.503	2.32E-05	0.005

Calibration Jet Pressures:

The yaw probes were calibrated over a range of ±40°. The pressures from each probe hole were recorded over this range. Pressure data was recorded over a time of 10 seconds. Figure 31 and Figure 32 show that there is slight fluctuations in Mach number during operation. These fluctuations can cause slight errors in probe readings. The Mach number is driven by the plenum pressure. As such, fluctuations in Mach number are driven by fluctuations in Plenum pressure. To address this the probe pressure readings are normalized based on the plenum pressure, shown below in Equation A5:

$$P_{Norm} = \frac{P_{probe}}{P_{Plenum}} \quad \text{(A5)}$$

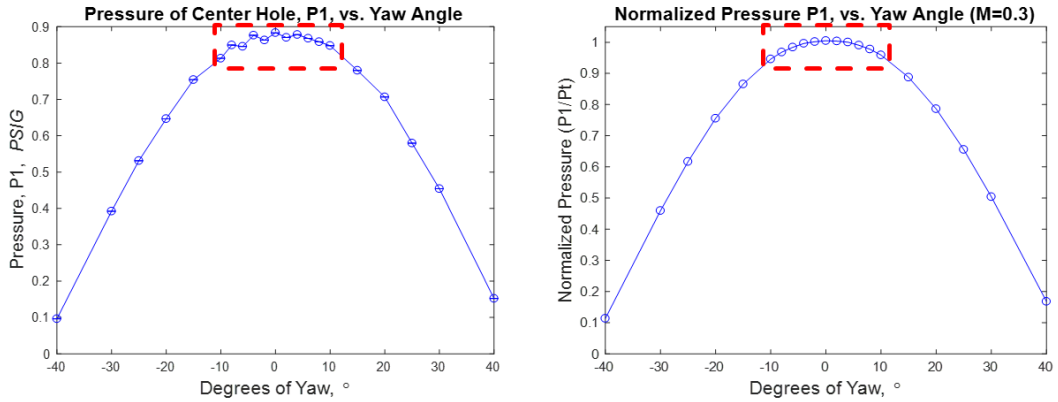

Figure 33. Smoothing Effect From Normalizing Pressure. Sample Taken From Cylindrical 55° P1 Hole.

Normalizing the pressure data made the data much smoother by accounting for slight Mach number fluctuations from the air compressor cycling or just slight errors during unsteady flow. The normalized pressures from each probe are shown in Figure 34 - Figure 43. 30° Wedge Probe calibrations had an error in the initial calibration for the perpendicular probe. Data from the parallel hole was mistakenly recorded for the perpendicular initial test. However, Test 1 had no sand deposition due to VTAR not reaching operating temperatures. As such, initial Perpendicular wedge probe data is omitted from the analysis, and Test 1 data is compared to subsequent tests. Comparing results from Parallel holes show that Test 1 had no impact on probe performance.

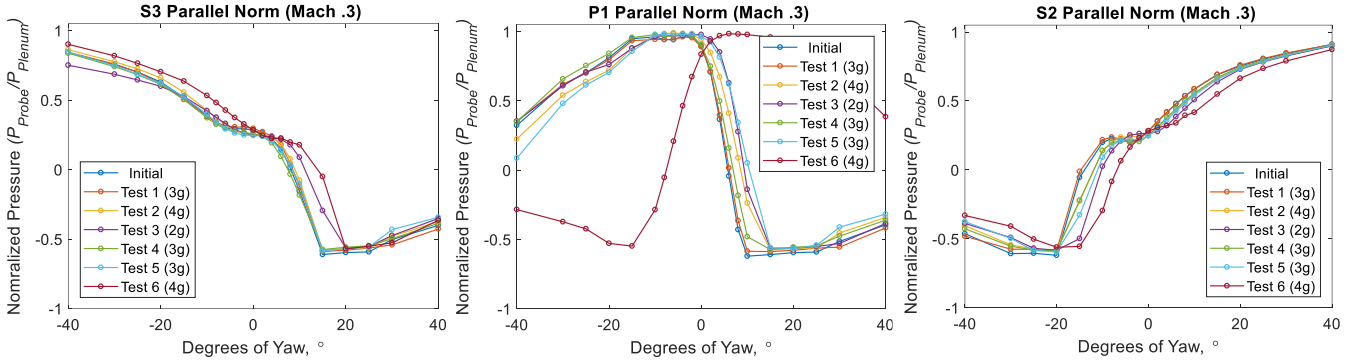

Figure 34. Parallel Wedge Probe: Mach 0.3 Normalized Pressure

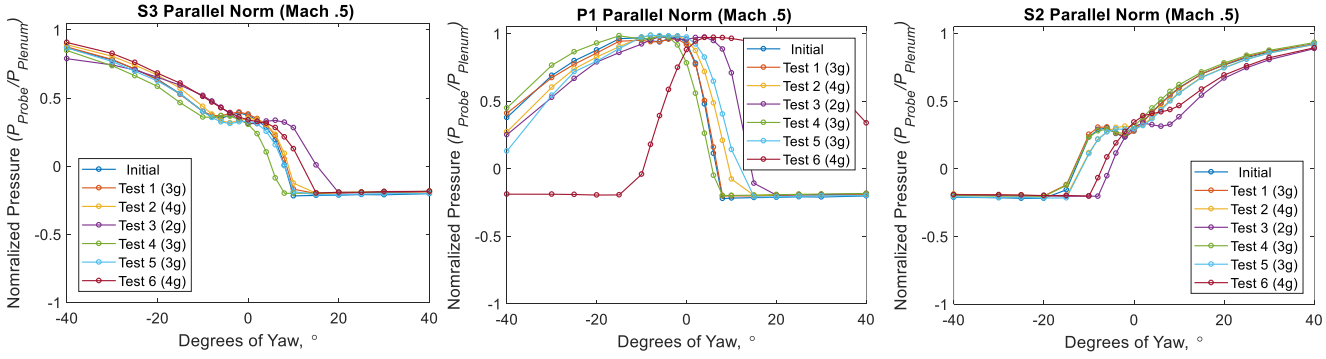

Figure 35. Parallel Wedge Probe: Mach 0.5 Normalized Pressure

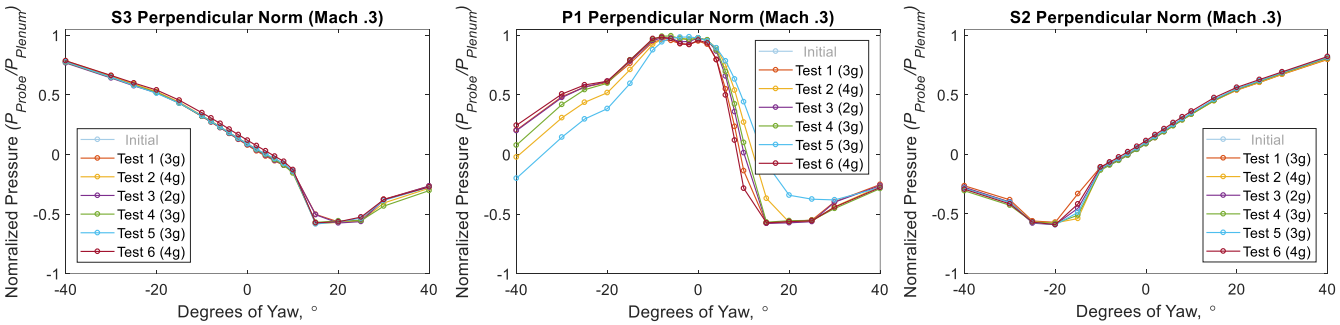

Figure 36. Perpendicular Wedge Probe: Mach 0.3 Normalized Pressure

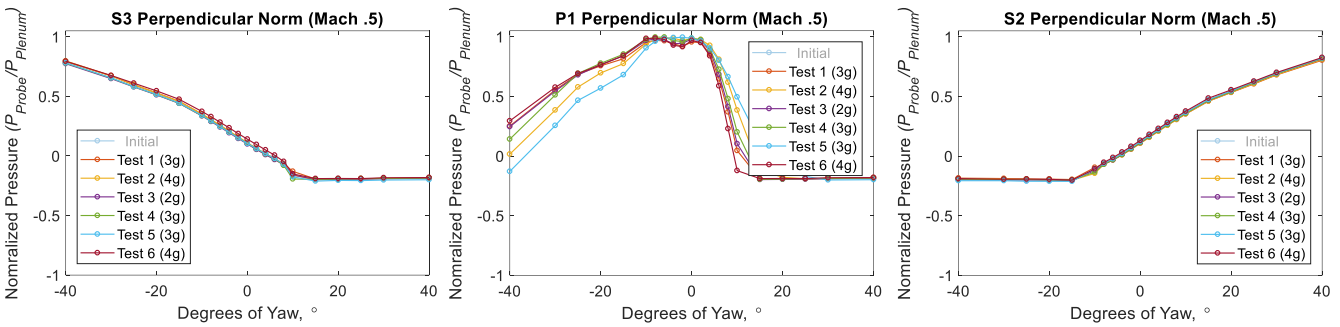

Figure 37. Perpendicular Wedge Probe: Mach 0.5 Normalized Pressure

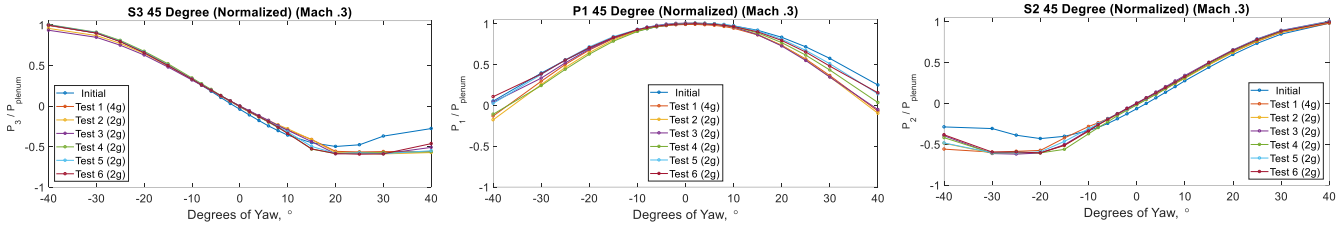

Figure 38. 45° Cylindrical Probe: Mach 0.3 Normalized Pressure

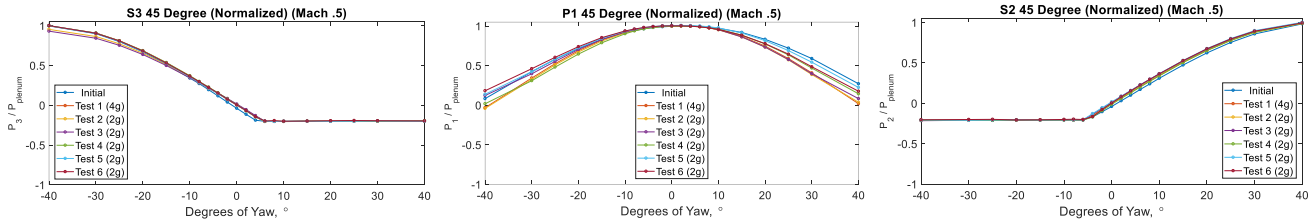

Figure 39. 45° Cylindrical Probe: Mach 0.5 Normalized Pressure

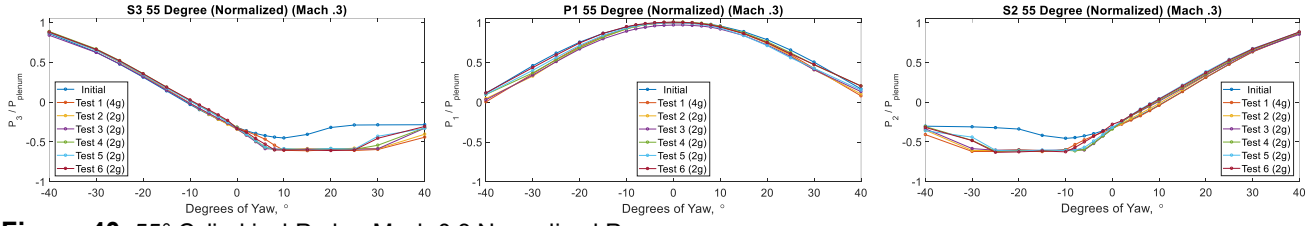

Figure 40. 55° Cylindrical Probe: Mach 0.3 Normalized Pressure

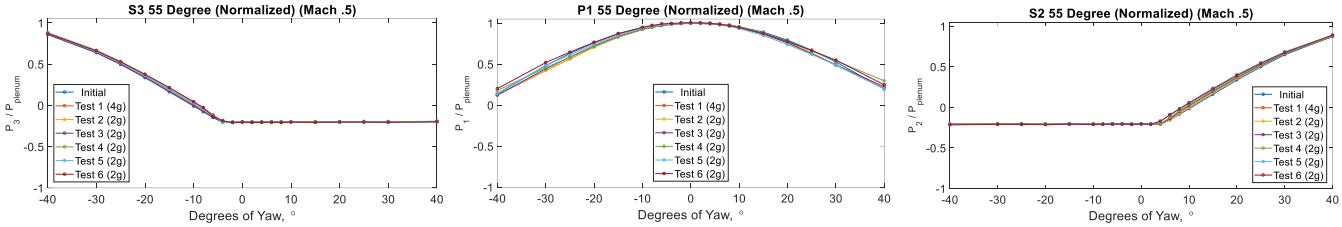

Figure 41. 55° Cylindrical Probe: Mach 0.5 Normalized Pressure

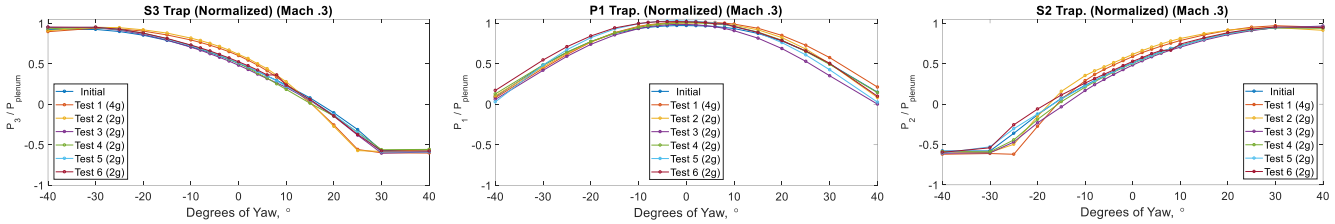

Figure 42. Trapezoidal Cylindrical Probe: Mach 0.3 Normalized Pressure

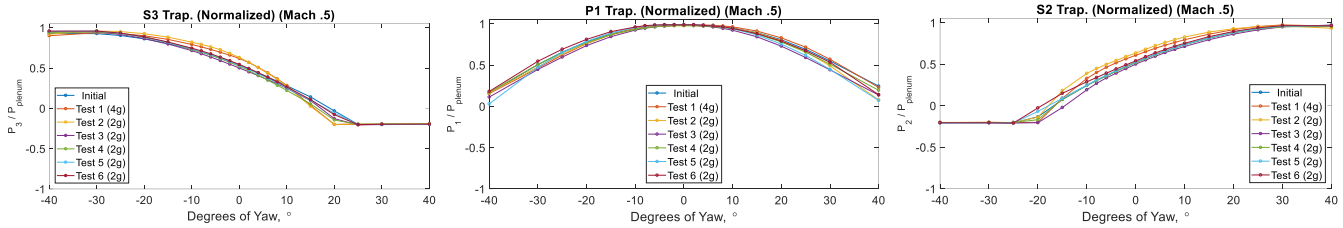

Figure 43. Trapezoidal Cylindrical Probe: Mach 0.5 Normalized Pressure

APPENDIX B. ARIZONA ROAD TEST DUST

Boulanger et. al [007] conducted deposition experiments using 20-40 µm ARD and found that sand deposition increased linearly as temperature increased from 975C to 1075C. Boulanger et al. [008] also found that temperature is the dominant mechanic in determining sand deposition. This trend is expected to be even more evident in smaller 0-5 µm particles, as they have less mass, and will heat up faster than the larger 20-40 µm particles.

Table 7 below shows the composition of Arizona road dust and the respective melting points of each of the components.

Table 7. Arizona Road Test Dust Composition

Components	Melting Pt	Quality
Silicon (Fine Dust)	1410 °C [2]	69-77%
Aluminum	660 °C [3]	8-14%
Iron	1538 °C [4]	4-7%
Calcium	850 °C [5]	2.5-5.5%
Potassium	65.3 °C [6]	2-5%
Sodium	97.8 °C [7]	1-4%
Magnesium	649 °C [8]	1-2%
Titanium	1668 °C [9]	0-1%

[15] K, Lux E. "Arizona Test Dust (ATD) Safety Data Sheet." Powdertechnologyinc.com, 4 Feb. 2016. http://www.powdertechnologyinc.com/wp-content/uploads/2012/08/SDS.01.Arizona-Test-Dust.4-Feb-2016-1.pdf

[16] "ICSC 0808 - QUARTZ," *ilo.org*, Nov-2016. [Online]. Available: http://www.ilo.org/dyn/icsc/showcard.display?p_version=2&p_card_id=0808. [Accessed: 20-Jun-2018].

[17] "ICSC 0988 - ALUMINIUM POWDER," Mar-2000. [Online]. Available: http://www.ilo.org/dyn/icsc/showcard.display?p_version=2&p_card_id=0988. [Accessed: 20-Jun-2018].

[18] *Lide, DR (ed.). CRC Handbook of Chemistry and Physics. 81st Edition. CRC Press LLC, Boca Raton: FL 2000, p. 4-64*

[19] "Calcium - Element information, properties and uses | Periodic Table," *Royal Society of Chemistry - Advancing excellence in the chemical sciences*. [Online]. Available: http://www.rsc.org/periodic-table/element/20/calcium. [Accessed: 20-Jun-2018].

[20] "Potassium - Element information, properties and uses | Periodic Table," *Royal Society of Chemistry - Advancing excellence in the chemical sciences*. [Online]. Available: http://www.rsc.org/periodic-table/element/19/potassium. [Accessed: 20-Jun-2018].

[21] "Sodium - Element information, properties and uses | Periodic Table," *Royal Society of Chemistry - Advancing excellence in the chemical sciences*. [Online]. Available: http://www.rsc.org/periodic-table/element/11/sodium. [Accessed: 20-Jun-2018].

[22] "ICSC 0289 - MAGNESIUM (POWDER)," *ilo.org*. [Online]. Available: http://www.ilo.org/dyn/icsc/showcard.display?p_version=2&p_card_id=0289. [Accessed: 20-Jun-2018].

[23] *Lide, DR (ed.). CRC Handbook of Chemistry and Physics. 81st Edition. CRC Press LLC, Boca Raton: FL 2000, p. 4-94*

APPENDIX C. UNCERTAINTY ANALYSIS

Table 8. Rotary Dial Instrument Uncertainty

Rotary Dial -Vexta Stepper Motor-B4800TS		
Accuracy[1]	100	arc-seconds
Accuracy[2]	0.03	deg
Resolution	0.025	deg
Deg/step	0.05	deg
Uncertainty	**0.08**	**deg**
Speed	100	deg/sec
Gear Ratio	18:01	

Table 9. Keller Valueline Pressure transducer Measurement Uncertainty

Pressure Transducer- Yaw Probe		
Keller Valueline High Accuracy Pressure Transmitter		
Range	5,10	psi
Accuracy [3]	0.25%	% Total Error Band(BR)
Accuracy	0.013	Psi
0-5 Uncertainty	**0.013**	**Psi**
0-10 Uncertainty	**0.025**	**Psi**

Power Supply Uncertainty

$$U_p = P \cdot \sqrt{\left(\frac{U_{VDC}}{VDC}\right)^2} = 5psi \cdot \sqrt{\left(\frac{0.48\,VDC}{24\,VDC}\right)^2} \qquad [D1]$$

Table 10. Transducer Power Supply Uncertainty

24 VDC Power Supply		
Range	24	VDC
Accuracy[4]	2%	
Accuracy	0.48	VDC
Accuracy	**0.1**	**Psi**

Combined Uncertainty

Table 11. Uncertainty In Normalized Pressure

Angle Uncertainty		
Rotary Dial	0.08	deg
Jet Mach Number Uncertainty		
Pressure	0.04	psi
Normalized Pressure Uncertainty		
Range	-1:1	P_norm
0-5 psi	0.020	P_norm
0-10 psi	0.021	P_norm

APPENDIX D. BLOCKAGE RATIOS FROM SAND FOULING AND CALIBRATION TESTING

Table 12. 30° Wedge Probe Blockage Ratios after sand fouling and after Calibration testing

			Test2_4g		Test3_3g		Test4_3g		Team5_3g		Team6_4g	
		Clean (Post Test 1)	Post Sand	Post Cal	Post Sand	Post Cal	Post Sand	Post Cal	Post Sand	Post Cal	Post Sand	Post Cal
		BLR (%)	BLR (%)	BLR (%)	BLR (%)	BLR (%)	BLR (%)	BLR (%)	BLR (%)	BLR (%)	BLR (%)	BLR (%)
Par	S2	0%	2%	0.7%	5.7%	1.9%	3.8%	3.6%	6.6%	5.7%	7.7%	0.6%
	P1	0%	61%	66.7%	57.8%	64.5%	63.2%	53.6%	77.1%	70.3%	89.8%	86.3%
	S3	0%	11%	11.6%	2.8%	10.0%	9.7%	9.8%	13.4%	14.1%	21.4%	20.8%
Perp	S2	0%	32%	32.7%	49.0%	34.3%	25.7%	21.6%	31.3%	29.2%	44.7%	37.9%
	P1	0%	51%	50.9%	44.2%	50.4%	43.1%	46.7%	65.8%	67.4%	91.2%	38.4%
	S3	0%	29%	22.8%	21.0%	24.5%	26.0%	16.3%	41.0%	33.7%	78.0%	63.2%

Table 13. Cylindrical Probe Blockage Ratios after sand fouling and after Calibration testing

			Test1_4g		Test2_2g		Test3_2g		Test4_2g		Test5_2g		Test6_2g	
		Clean (Initial)	Post Sand	Post Cal	Post Sand	Post Cal	Post Sand	Post Cal	Post Sand	Post Cal	Post Sand	Post Cal	Post Sand	Post Cal
		BLR (%)	BLR (%)	BLR (%)	BLR (%)	BLR (%)	BLR (%)	BLR (%)	BLR (%)	BLR (%)	BLR (%)	BLR (%)	BLR (%)	BLR (%)
45°	P1	0%	67%	68%	77%	77%	85%	86%	92%	86%	59%	59%	70%	63%
	S2	0%	40%	37%	49%	50%	53%	51%	28%	22%	49%	52%	58%	61%
	S3	0%	38%	36%	32%	21%	27%	26%	32%	31%	34%	32%	42%	34%
55°	P1	0%	64%	63%	73%	59%	69%	73%	81%	68%	77%	67%	76%	71%
	S2	0%	23%	16%	25%	27%	23%	25%	17%	14%	23%	16%	23%	23%
	S3	0%	21%	20%	26%	17%	15%	14%	20%	27%	19%	19%	34%	19%
Trap	P1	0%	33%	31%	60%	61%	68%	69%	69%	67%	70%	69%	76%	70%
	S2	0%	53%	51%	73%	71%	89%	26%	31%	23%	31%	0%	20%	17%
	S3	0%	70%	71%	78%	77%	90%	32%	30%	8%	16%	7%	34%	31%